Supporting Material

Pattern selection by dynamical biochemical signals

David Palau-Ortin[1], Pau Formosa-Jordan[1,2], José M. Sancho[1], Marta Ibañes[1,*]
[1] Departament d'Estructura i Constituents de la Matèria, Facultat de Física, Universitat de Barcelona. Martí i Franquès, 1. 08028 Barcelona, Spain.
[2] Current address: Sainsbury Laboratory, University of Cambridge, Bateman Street, Cambridge, CB2 1LR, United Kingdom.
∗ E-mail: mibanes@ub.edu

This supporting material contains 15 figures and 3 tables with the corresponding captions.

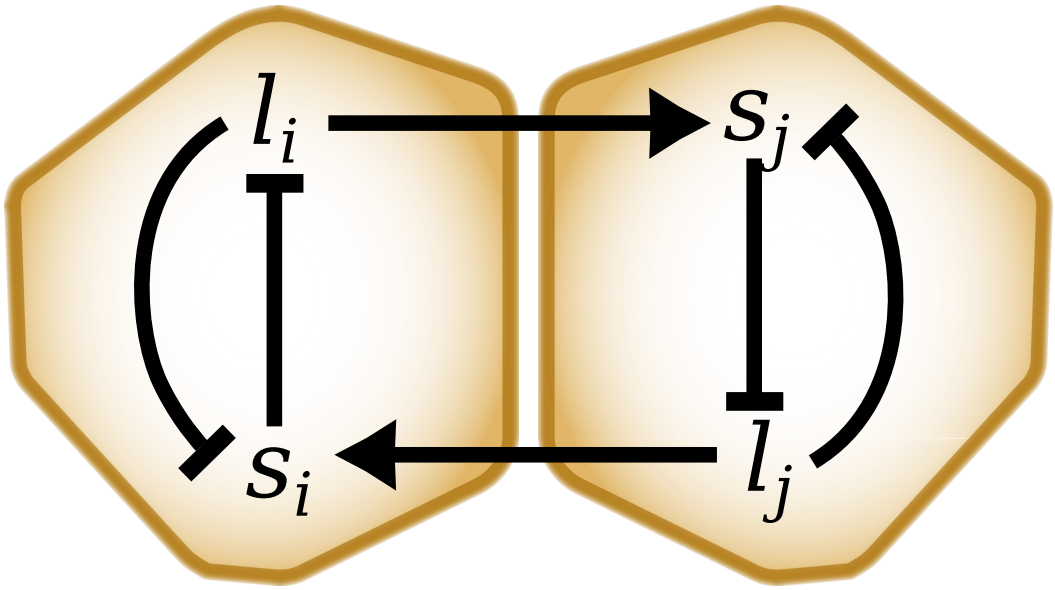

FIGURE S1: **Scheme of the model interactions between two adjacent cells.** Ligand activity in cell i (l_i) induces (*arrow*) Notch activity in the adjacent cell j (s_j) and inhibits (*blunt arrow*) Notch activity in cell i (s_i). In turn, s_i inhibits (*blunt arrow*) l_i. The reciprocal interactions in cell j are also depicted.

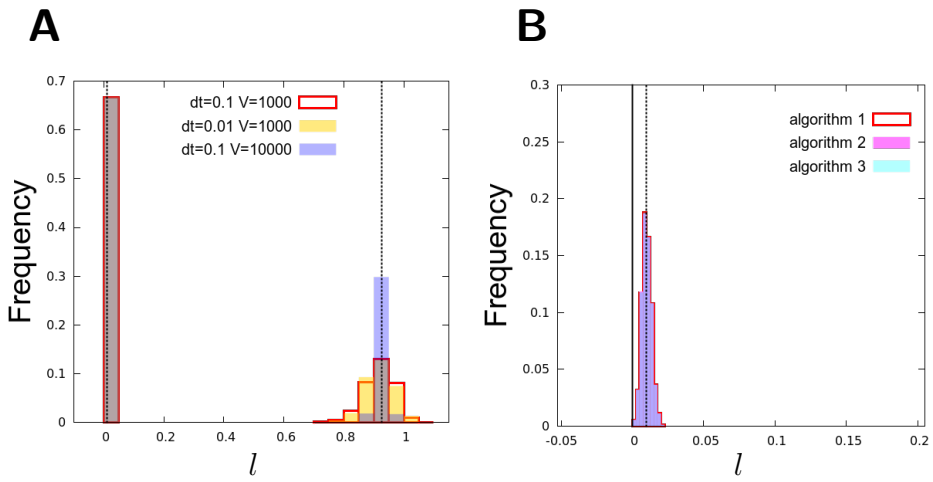

FIGURE S2: **The stochastic implemented algorithm is consistent with the theoretical deterministic predicted values.** Histograms of the ligand activity values (l_i) in a lattice of $N = 48\times48$ cells with periodic boundary conditions at the steady state ($t = 10000$). Initially ($t = 0$) the lattice starts with the perfect pattern solution theoretically predicted for the deterministic dynamics (values denoted by *dashed vertical lines*) for $r_t = 1.0$ and $r_c = 0.1$, $b = 1000$ and $n = 2$. (A) Histograms for different values of V and time integration step dt. In the model, the intensity of fluctuations depends on $1/V$. The mean values are in agreement with the theoretical predictions. (B) Due to the multiplicative noise, the variables might reach negative values. The algorithm implemented in the simulations presented in all figures corrects it by fixing the variable to zero when it is going to become negative (*algorithm 1*, in *open red boxes*). We compared the results obtained by this algorithm with those arising from two different algorithms: with a reflective barrier in zero (i.e., the negative values are converted into their positive counterpart; *algorithm 2*, in *cyan boxes*) or without any correction (i.e. negative values exist; *algorithm 3*, in *magenta boxes*). The three distributions are very similar. The solid vertical line is depicted to denote the zero ligand activity value. Simulations of the three algorithms have been generated with $V = 1000$.

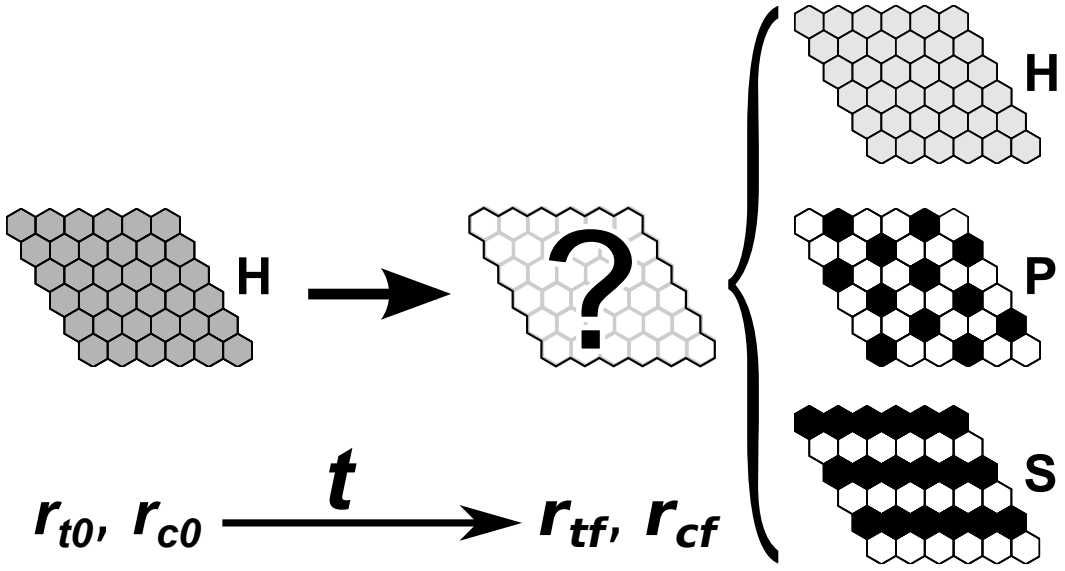

FIGURE S3: **Cartoon exemplifying the problem of pattern selection**. Initially, the system is in a stable homogenous (H) pattern determined by the initial value of the control parameters (r_{t0}, r_{c0}). These parameters evolve over time (t) to final values (r_{tf}, r_{cf}) due to the action of biochemical signals. At these new values of the parameters, there are multiple patterns which are all stable, for instance, the homogeneous (H), a periodic salt-and-pepper (P) and a stripped (S) pattern. The problem tackled here is how to select one of these patterns. We considered three different scenarios, which can select different types of patterns, according to how the parameters change over time and across the tissue. The figure exemplifies the selection from an initial monostable H pattern. Other initial conditions involving multistability are explored too.

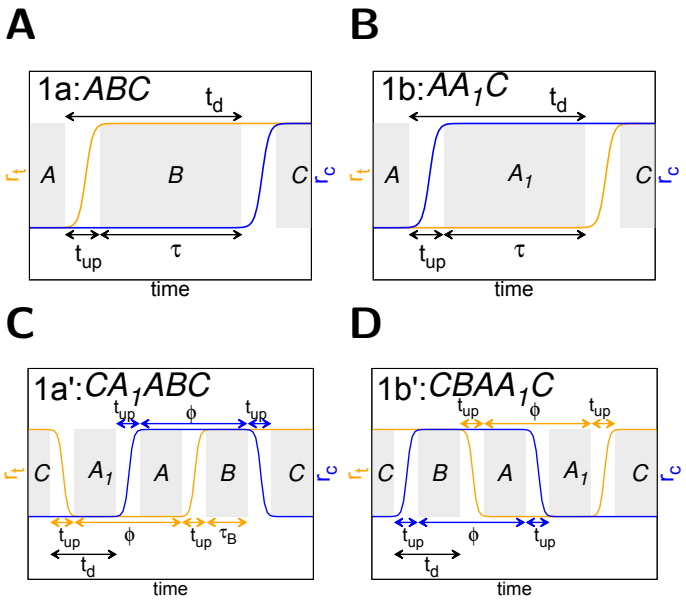

FIGURE S4: **Parameter changes for the different paths in scenario 1.** Changes of r_t (orange) and r_c (blue) along time for the different paths in scenario 1: (A) path 1a, (B) path 1b, (C) path 1a' and (D) path 1b'. The parameter space points that characterize each path are depicted (see Fig. 1, A-B). The time period spent by the system in each of these points is shadowed in grey (e.g., τ_B for B). Parameters defining the time scale dynamics (t_{up}, τ, t_d and ϕ) of the parameter changes are also depicted. (A and B) Paths 1a and 1b share the same initial and final parameter space points, but they differ in the parameter space points visited along time. In path 1a, r_t changes first and then r_c. The opposite order happens in path 1b. (C and D) Paths 1a' and 1b' are cyclic (the end coincides with the start) and share the same parameter space points visited. Paths 1a' and 1b' only differ in the temporal sequence. In path 1a', r_t changes first and then r_c changes. The reverse order happens in path 1b'. Notice that the examples shown correspond to changes which involve the same values of ϕ and t_{up} for r_c and r_t.

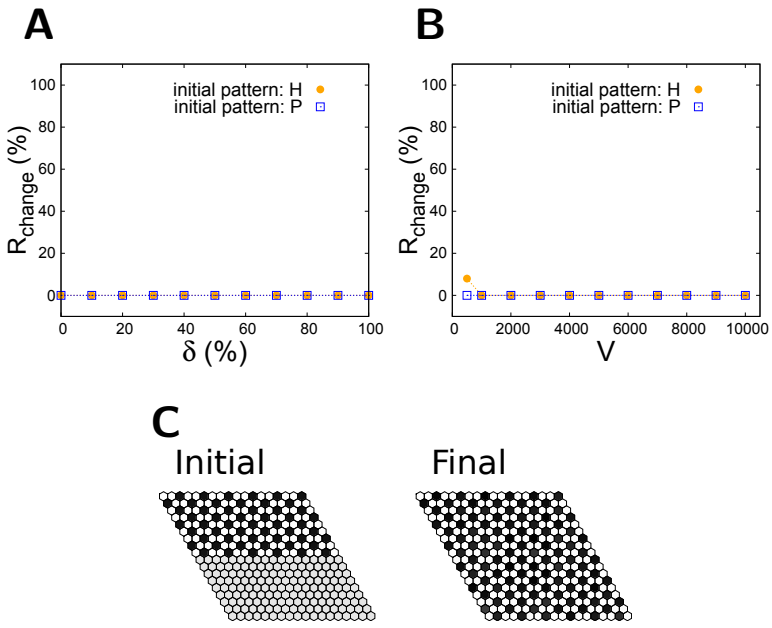

FIGURE S5: **Numerical stability analysis of the H and P patterns at point C in the parameter space of Fig. 1A, 1B, 3A and 3B ($n = 2$).** (A and B) Percentage of simulations that reach a steady pattern at $t = 200$ that is distinct from the initial pattern in the absence of any biochemical signal for (A) deterministic dynamics and (B) stochastic dynamics. (A) Both the H (orange circles) and P (blue squares) patterns are deterministically stable for a large range of amplitudes δ of random initial perturbations. Initial conditions are $s_i(t=0) = s_{0i}\,(1+\delta\ \ (2\,r-1))$ and $l_i(t=0) = l_{0i}\,(1+\delta\ \ (2\,r-1))$, where r is a uniformly distributed random number within $[0,1]$, and s_{0i} and l_{0i} are the theoretical predicted values of s_i and l_i, respectively of the pattern being analyzed. (B) Both the H (*orange circles*) and P (*blue squares*) patterns are stochastically stable. Initial conditions as in panel A with $\delta = 0$. The initial pattern remains at the end of the simulation for a wide range of V values (except for the H pattern for very large fluctuations with $V = 500$). The percentages in panels A and B (R_{change}) have been obtained with 1000 simulations for each δ and V value. (C) Relative spatial stability of the H and P patterns. (*Left*) Initial condition with the top half of the tissue in the P pattern (with the theoretical predicted values) and the other bottom half in the H pattern (with the theoretical predicted values). (*Right*) Steady state reached after numerical integration of the stochastic dynamics for $V = 1000$ with the initial condition shown in left panel. The P solution invades all the tissue. In all panels, parameter values of point C of Fig. 1A, 1B, 3A and 3B ($r_t = 1.0$, $r_c = 0.1$, $b = 1000$, $n = 2$), and periodic boundary conditions were used.

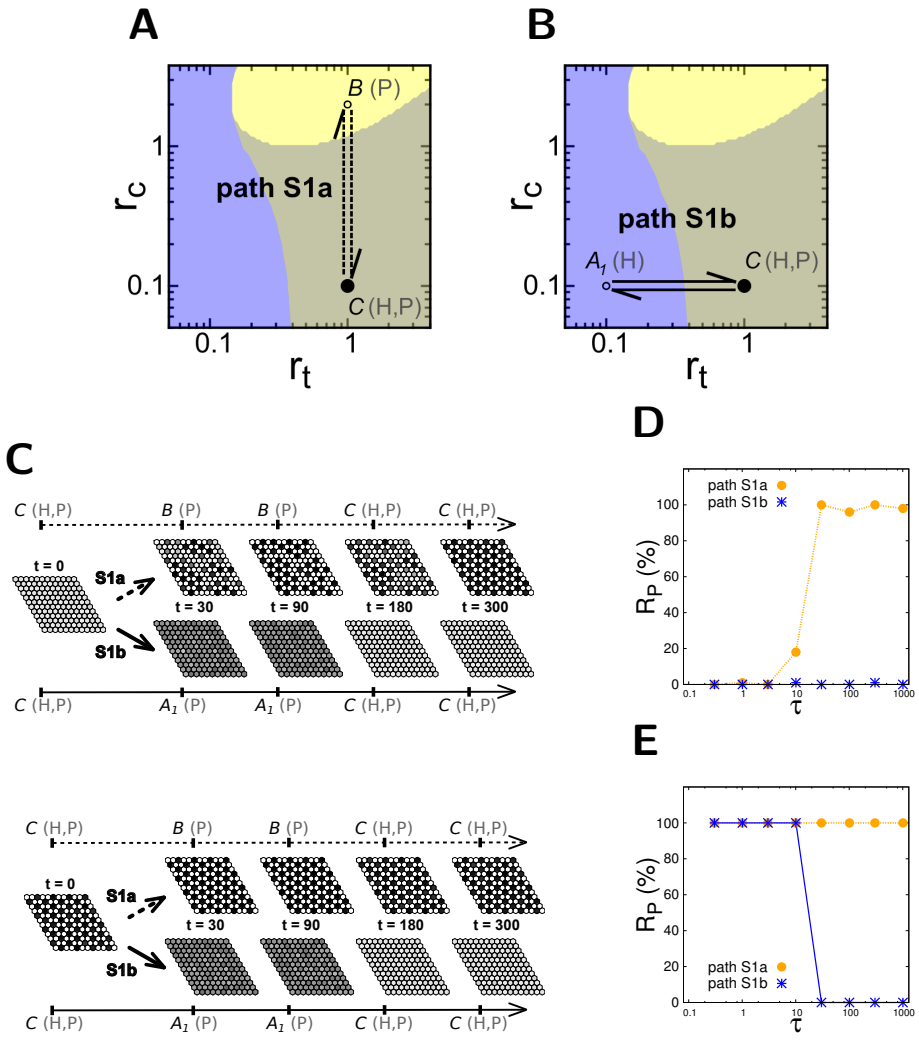

FIGURE S6: **Selection of a new pattern requires transient destabilization of the initial pattern.** (A and B) Paths (*arrows*) S1a (A) and S1b (B) in the same parameter space as in Fig. 1,A-b, and fig 3,A-B. (*Solic circles*) Initial and final points of the patterns; (*open circles*) intermediate vertex points. Notice that these two trajectories on the parameter space are produced by biochemical signals that transiently change either the control parameters r_t or r_c in all cells at the same time (see Fig. S9). (C) Snapshots of the state of the system over time for each path and for initial condition being the (*top*) H or (*bottom*) P pattern, for $\tau = 90$. The initial, intermediate path vertex and final points of each path and the time t of each snapshot are indicated. The results show that the selection of a pattern different from the initial one only occurs when the path involves a transient destabilization of the initial pattern. (D and E) Percentage of selection of P pattern (R_P) versus τ when the initial state is H (D) and when the initial state is P (E). Different colors and symbols are used to distinguish selections from each path (path S1a in *orange circles*, and path S1b in *blue stars*), as indicated. Notice that selection of a new pattern requires a minimal time (τ). Other parameter values as in Fig. 1 and in Table S1.

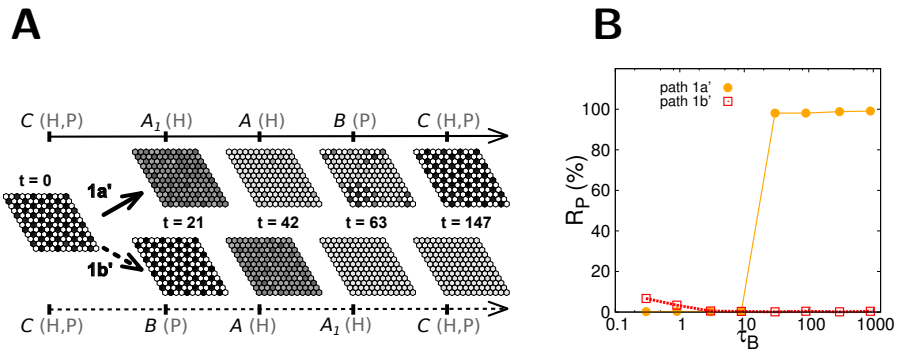

FIGURE S7: **Selection through paths 1a' and 1b' when the initial state is the P pattern.** (A) Snapshots of the tissue state over time (t) when the system initially ($t = 0$) exhibits the P pattern, for path 1a': CA_1ABC and path 1b': $CBAA_1C$, with $\tau_{A1} = \tau_A = \tau_B = 10$. These cyclic paths are depicted in Fig. 1B. The results corresponding to these same paths but when the system initially exhibits the H pattern are shown in Fig. 1D. (B) Frequency of selection of the P pattern (R_P in percentage) versus the time spent at each intermediate vertex point of the parameter space ($\tau_{A1} = \tau_A = \tau_B$) when the initial pattern is P, for paths 1a' and 1b'. The results corresponding to these same paths but when the system initially exhibits the H pattern are shown in Fig. 2B. Parameter values in panels A and B as in Figs. 1D and 2B, respectively.

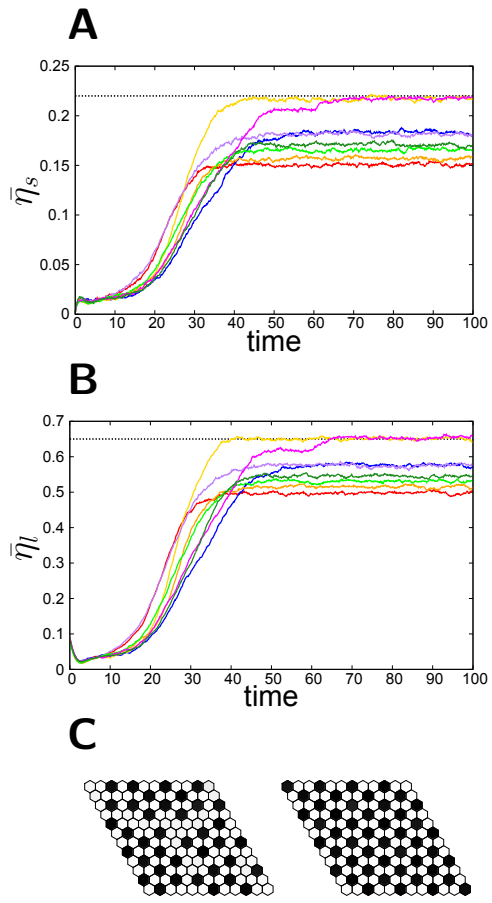

FIGURE S8: **Stochastic time evolution of order parameters during pattern P formation**. (A and B) Eight different stochastic time evolutions of order parameters $\bar{\eta}_s$ (A) and $\bar{\eta}_l$ (B) as defined in Materials and Methods, for the parameter values of parameter space point B of Figs. 1, A-B, and 3, A-B ($r_t = 1.0$, $r_c = 0.1$). The initial condition is the H pattern with the theoretical predicted values of s and l of the homogeneous stable state of point A in the parameter space ($r_t = 0.1$,$r_c = 2.0$). The dashed line stands for the predicted theoretical value of the order parameter for a perfect periodic deterministic stationary pattern (see the value in Table S1). (C) Pattern at time $t = 100$ for the red (*left*) and yellow (*right*) trajectories of panels A and B. These patterns are stationary. According to panels A and B, the characteristic time to form the P pattern in point B of parameter space is $T \sim 40 - 50$ (see Table S2 for the average values of T, with more volumes and tissue sizes explored). Moreover, the final stationary states are different because the final pattern is not perfectly periodic in all the tissue. Other parameters of the simulation are: $V = 1000$, $b = 1000$, $n = 2$.

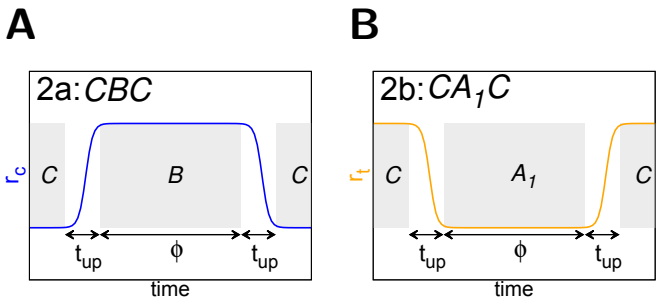

FIGURE S9: **Parameter changes for the different paths in scenario 2.** Changes of r_t (*orange*) and r_c (*blue*) along time for the different paths in scenario 2: (A) path 2a, (B) path 2b. The parameter space points that characterize each path (see Fig. 3, A-B) are depicted. The time period spent by the system in each of these points is shadowed in grey (e.g., τ_B for B). Parameters defining the time scale dynamics (t_{up} and $\phi = \tau$) of the parameter changes are also depicted. (A and B) Paths 2a and 2b are cyclic and parameter changes only occur for a subset of cells. Paths 2a and 2b differ in the parameter that is changed along the path (r_c in path 2a, and r_t in path 2b) while the other one remains constant. Hence, these paths differ in the parameter space point transiently visited (B in path 2a, and A_1 in path 2b).

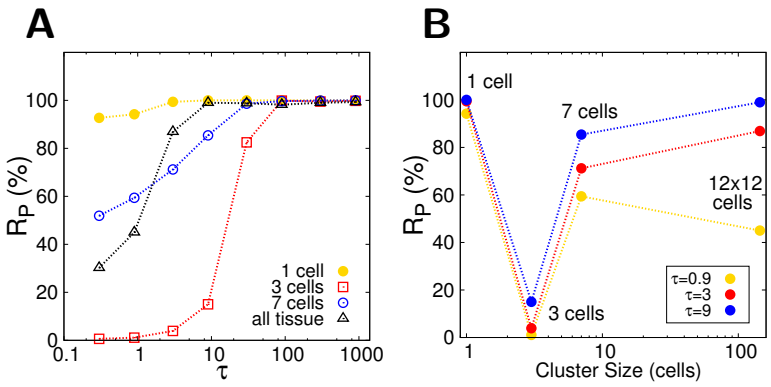

FIGURE S10: **Selection by a cyclic path that acts only on a cluster of cells (scenario 2)**. The cyclic path used herein involves transient changes of the parameter values as those depicted for path 1a' in Fig. 1B and S4C. The path starts and ends at point C of the parameter space of Fig. 1B. The changes of the parameter values only occur on a subset of cells, while the rest of the cells of the tissue remain at all time with the parameter values of point C. This is in contrast with path 1a' which acts upon all cells of the tissue. (A) Frequency of selection of the P pattern (R_P in percentage) for 1000 repetitions versus the time spent at each intermediate parameter space vertex point of the path τ ($\tau = \tau_B = \tau_{A1} = \tau_A$). The signal drives the change of the control parameters only in the number of cells detailed in the legend, located at the centre of the tissue. (B) The same results as in panel A but depicted as a function the number of cells that change their parameter values. Different curves correspond to different τ values (see the legend). Notice the non monotonous dependency of the pattern selection with the cluster size for this path. Other parameter values as in Fig. 2B. The total size of the tissue is 12×12.

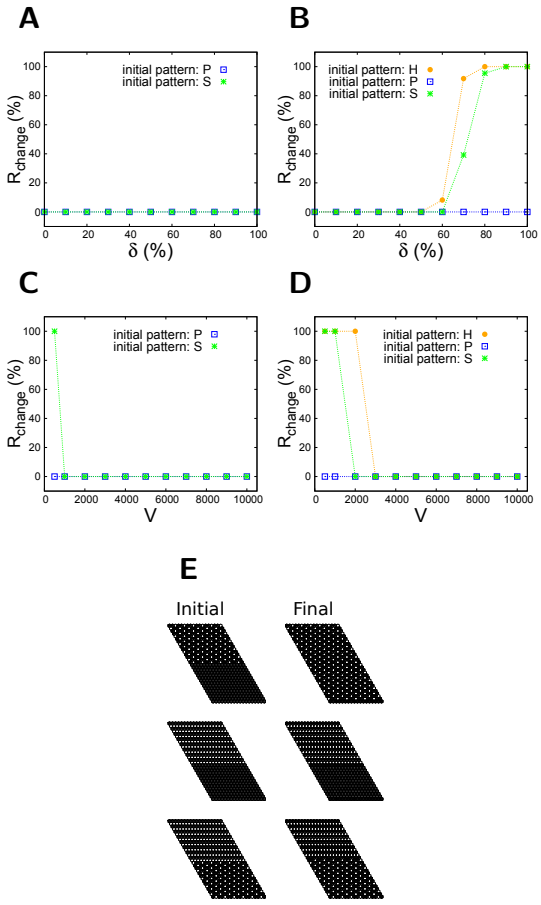

FIGURE S11: **Numerical stability analysis of the H, P and S patterns at points *B* and *C* in the parameter space of Fig. 5A ($n = 4$).** (A-D) Percentage of simulations that reach a steady pattern at $t = 200$ that is distinct from the initial pattern in the absence of any biochemical signal for (A and B) deterministic dynamics and (B and C) stochastic dynamics for the parameter values of point B (A and C) and C (B and D) of the parameter space of Fig. 5A. (A and B) Stability for deterministic dynamics for different amplitudes of initial random perturbations of the theoretical predicted patterns. The initial conditions are $s_i(t=0) = s_{0i}\,(1+\delta\ \ (2\,r-1))$ and $l_i(t=0) = l_{0i}\,(1+\delta\ \ (2\,r-1))$, where r is a uniformly distributed random number within $[0,1]$, and s_{0i} and l_{0i} are the theoretical predicted values of s_i and l_i, respectively of the pattern being analyzed. (C and D) Stability for stochastic dynamics with different V values for initial conditions being the theoretical predicted patterns ($\delta = 0$). Notice that for the value of V used in the simulations of scenario 3 ($V = 10000$) all the pattern solutions are stochastically stable. The percentages shown in panels A-D (R_{change}) have been obtained with 1000 simulations for each δ and V value. (E) Relative spatial stability of the H, P and S patterns at point C in the parameter space of Fig. 5A. (*Left*) Initial tissue with: (*top*) half of the cells in the P pattern and the other half in the H pattern; (*middle*) half of the cells in the stripped S pattern and the other half in the P pattern; (*bottom*) half of the cells in the P pattern and the other half in the S pattern (*bottom*). Theoretical predicted values for the H, P and S solutions were used. (Right) Steady state reached after numerical integration of the stochastic dynamics for $V = 10000$ with the initial condition shown in left panel. If the initial condition is the P and S patterns in contact through a black stripe, this stripe is invaded by the P pattern (data not shown). In all panels, parameter values and boundary conditions as in Fig. 5.

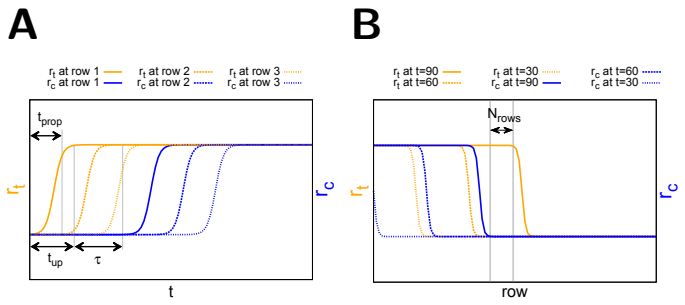

FIGURE S12: **Parameter changes for the different paths in scenario 3.** (A) Temporal evolution of the r_t (*orange*) and r_c (*blue*) parameters for different rows of the tissue, as indicated. τ stands for the time period during which a row is at the intermediate vertex point, B, of the path. t_{prop} is the time required for the parameter to change from one row to the adjacent one. (B) Spatial distribution of the r_t (*orange*) and r_c (*blue*) parameters at different times, as indicated. N_{rows} is the number of rows that are at the same intermediate vertex point of the path 3. The parameter values explored by the path are depicted in Fig. 5A and in Table S3.

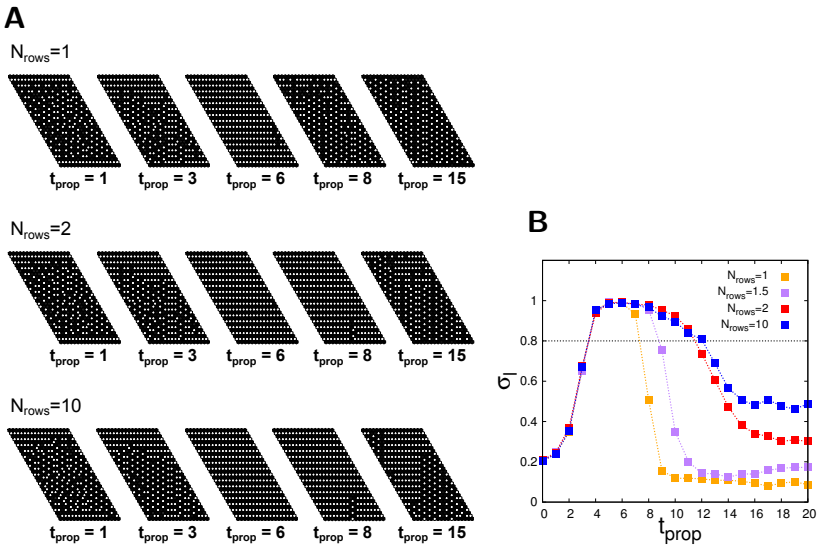

FIGURE S13: **Selection of the S pattern requires a path with optimal spatiotemporal dynamics.** (A) Snapshots of the stationary state reached through path 3 in Fig. 5, A-B, for different spatiotemporal dynamics of the path, i.e., different values of t_{prop} and N_{rows} (Materials and Methods, Fig. S12). The initial condition is the H pattern of point A in parameter space of Fig. 5A. The S pattern is selected only for a range of optimal t_{prop} values which slightly enlarges with N_{rows}, as Fig. 6 shows (averaging different repetitions). For very short t_{prop} values, the parameter change propagates almost instantaneously across the tissue and hence the results for homogeneous (spatially independent) changes of the parameter values is recovered (pattern P is selected). For large values of t_{prop}, the P pattern is selected too. (B) Values of σ_l (average of 100 repetitions) for path 3 versus t_{prop} (propagating time). Results for different number of cell rows being simultaneously at point B of the path (N_{rows}, see legend) are shown. The dashed line points out the value of 0.8, which has been considered as a threshold for stripes selection (R_S). See the definition of σ_l in Material and Methods section. Other parameter values and boundary conditions as in Figs. 5 and 6.

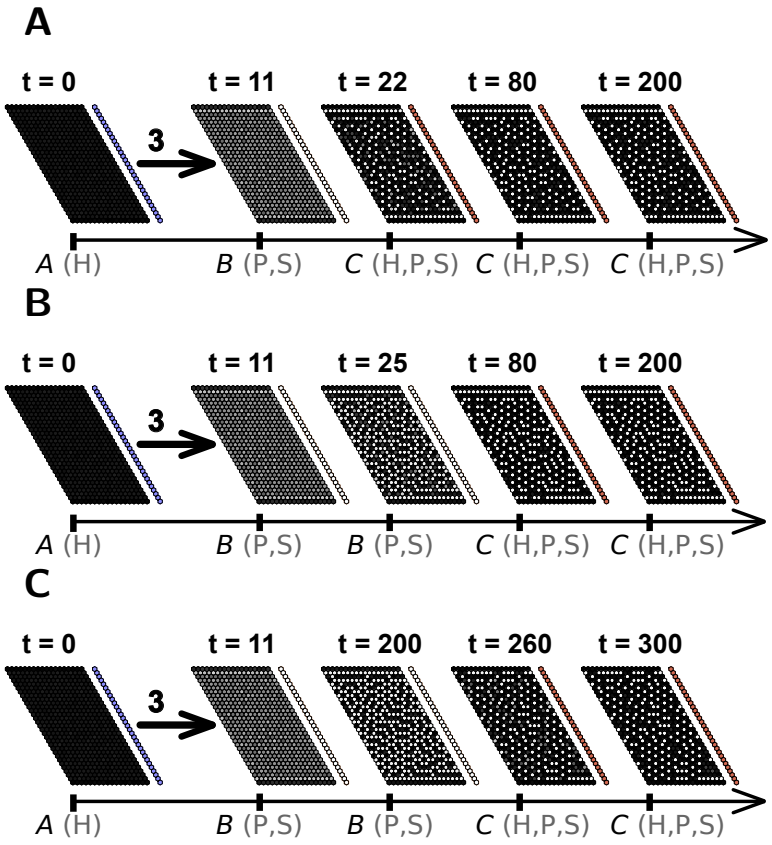

FIGURE S14: **Pattern selection achieved through path 3 with $t_{prop} = 0$.** Snapshots of the tissue state over time (t) when the system starts ($t = 0$) with the homogeneous H pattern and parameters change over time according to path 3 in Fig. 5A but with $t_{prop} = 0$. Therefore, all cells change their parameter values at the same time. In these cases, path 3 (with $t_{prop} = 0$) is of the scenario 1-like type. The column of colored cells at the right of each panel shows the point of the parameter space (Fig. 5A) at which each cell row is (*blue* for point A, *white* for B and *red* for C). Three values of τ have been explored. (A) The tissue spends no time in B parameter space point, so $\tau = 0$. (B) Each cell of tissue spends as much time in B as a cell does in the path studied in Fig. 5C. It uses $\tau = 14$. (C) The whole tissue spends as much time in B ($\tau = 231$) as the tissue in Fig. 5 remains with at least one row of cells in B. Notice that for these three values of τ (A-C), the S pattern is not selected. Other parameter values and boundary conditions as in Fig. 5.

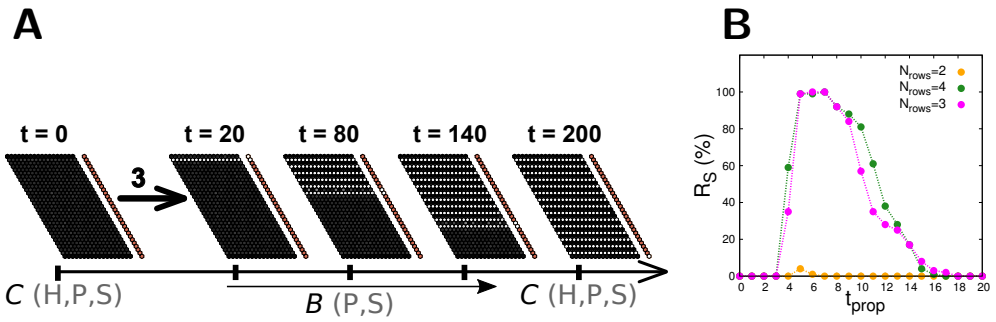

FIGURE S15: **Selection of the S pattern through transient spatio–temporal changes of the parameter values.** (A) Snapshots of the tissue state over time (t) when the system starts and ends up at the same parameter space point C and transiently visits parameter space point B of Fig. 5A. We have named this path as path S3. Parameters change according to a path 3-like, i.e. propagating from top to bottom cell rows (like in Fig. 5B for path 3). The column of colored cells at the right of each panel shows the point of the parameter space at which each cell row is (*white* for B and *red* for C). Parameter values are $t_{prop} = 6$, $N_{rows} = 4$. The system initially ($t = 0$) exhibits the H pattern. (B) Frequency of selection of the S pattern (R_S in percentage) for the path described in panel A versus t_{prop} for 100 repetitions. Results for different number of cell rows being simultaneously at point B of the path (N_{rows}, see legend) are shown. Parameter values and boundary conditions as in Fig. 5C.

Points	$\mathbf{r_t}$	$\mathbf{r_c}$	**Patt**	$\boldsymbol{s^{st}}$ (Δs^{st})	$\boldsymbol{l^{st}}$ (Δl^{st})	$\boldsymbol{\bar{\eta}_s^{th}}$	$\boldsymbol{\bar{\eta}_l^{th}}$
A	0.1	2.0	H	0.027 (±0.007)	0.6 (±0.1)	0.00	0.00
A_1	0.1	0.1	H	0.038 (±0.007)	0.41 (±0.07)	0.00	0.00
B	1.0	2.0	P	0.32 (±0.02), 0.003 (±0.002)	0.009 (±0.003), 0.99 (±0.03)	0.22	0.65
C	1.0	0.1	H	0.09 (±0.01)	0.10 (±0.02)	0.00	0.00
			P	0.32 (±0.02), 0.009 (±0.003)	0.010 (±0.003), 0.93 (±0.05)	0.21	0.61

TABLE S1: **Parameter and order parameter values for different points of the parameter space shown in Figs. 1A, 1B, 3A and 3B with $n = 2$.** The fourth column (*Patt*) shows which of the studied pattern solutions are stable for the parameter values (*Points*, first column) of r_t, r_c (second and third columns; see them depicted in the parameter space in Figs. 1, A-B, and Fig. 3, A-B). s^{st} and l^{st} are the theoretical stationary deterministic values of each cell type for each pattern. Δs^{st} and Δl^{st} are the fluctuation amplitude. These amplitudes have been obtained by computing the standard deviation of the final states of the cells in a tissue of 48×48 cells, when the stochastic dynamics of Eqs. 1-2 are considered with $V = 1000$. $\bar{\eta}_s^{th} = \frac{\eta_s^0+\eta_s^-+\eta_s^+}{3}$ and $\bar{\eta}_l^{th} = \frac{\eta_l^0+\eta_l^-+\eta_l^+}{3}$ are the theoretical deterministic values of the order parameters as defined in Materials and Methods for the different stable solutions. Other parameters: $b = 1000$ and $n = 2$; and final time $t = 100$ for the numerical simulations.

A

V	Size	T
100	12×12	38 ± 6
1000	6×6	58 ± 18
1000	12×12	54 ± 5
1000	24×24	54 ± 2
10000	12×12	73 ± 7

B

Size	T
12×12	103 ± 16
3 cells	73 ± 14

TABLE S2: **Characteristic time, T, for pattern formation in point B of Figs. 1A, 1B, 3A and 3B.** Tables showing the average characteristic time T of P pattern formation and its standard deviation for (A) stochastic dynamics and (B) deterministic dynamics for the parameter values of point B of Table S1 (Fig. 1, A-B, and Fig. 3, A-B). The initial condition is the H pattern solution at parameter space point A of Fig. 1, A-B, and Fig. 3, A-B. T is defined as the time at which the order parameters $\bar{\eta}_s$ and $\bar{\eta}_l$ reach 90% of their stationary values each. The stationary values of the order parameters (for $x = s, l$) were computed as the time-averaged values of $\bar{\eta}_x(t)$ over a period $\Delta t = 10$ during which the standard deviation of $\bar{\eta}_x(t)$ is less than 0.01 times the time-average value. In B, the initial condition is the H pattern of parameter space point A of Fig. 1, A-B, with a random perturbation of amplitude $\delta = 10\%$.

Path points	$\mathbf{r_t}$	$\mathbf{r_c}$	**Patterns**	$\bar{\eta}_s^{th}$	$\bar{\eta}_l^{th}$	$(\eta_s^0, \eta_s^-, \eta_s^+)^{th}$	$\left(\eta_l^0, \eta_l^-, \eta_l^+\right)^{th}$
A	0.5	3.4	H	0.00	0.00	$(0.00, 0.00, 0.00)$	$(0.00, 0.00, 0.00)$
B	1.3	3.4	P	0.23	0.63	$(0.00, 0.00, 0.00)$	$(0.00, 0.00, 0.00)$
			S	0.22	0.60	$(0.00, 0.33, 0.33)$	$(0.00, 0.90, 0.90)$
C	1.3	8.6	H	0.00	0.00	$(0.00, 0.00, 0.00)$	$(0.00, 0.00, 0.00)$
			P	0.32	0.65	$(0.32, 0.32, 0.32)$	$(0.65, 0.65, 0.65)$
			S	0.23	0.64	$(0.00, 0.35, 0.35)$	$(0.00, 0.96, 0.96)$

TABLE S3: **Parameter and order parameter values for different points of the parameter space shown in Fig. 5A with $n = 4$.** The "Patterns" column shows which of the studied pattern solutions are stable for the parameter values r_t, r_c (see them in the parameter space in Fig. 5A). $\bar{\eta}_s^{th} = \frac{\eta_s^0 + \eta_s^- + \eta_s^+}{3}$ and $\bar{\eta}_l^{th} = \frac{\eta_l^0 + \eta_l^- + \eta_l^+}{3}$ are the theoretical deterministic values of the order parameters for the different stable solutions. $\left(\eta_s^0, \eta_s^-, \eta_s^+\right)$ and $\left(\eta_l^0, \eta_l^-, \eta_l^+\right)$ are the theoretical three-component order parameters for the different solutions. Notice that we have shown a certain direction (among three possible directions in the cell lattice) for the stripes.